HHS Public Access

Author manuscript

Biochim Biophys Acta Mol Basis Dis. Author manuscript; available in PMC 2021 January 01.

Published in final edited form as:

Biochim Biophys Acta Mol Basis Dis. 2020 January 01; 1866(1): 165580. doi:10.1016/j.bbadis.2019.165580.

TDP-43 inhibitory peptide alleviates neurodegeneration and memory loss in an APP transgenic mouse model for Alzheimer's disease

Ju Gao[a,1], **Luwen Wang**[a,1], **Chao Gao**[a,1], **Hiroyuki Arakawa**[b], **George Perry**[c], **Xinglong Wang**[a,d,*]

[a]Department of Pathology, Case Western Reserve University, Cleveland, OH, USA.

[b]Department of Anatomy and Neurobiology, University of Maryland School of Medicine, Baltimore, MD, USA

[c]College of Sciences, University of Texas at San Antonio, San Antonio, TX, USA.

[d]Center for Mitochondrial Diseases, Case Western Reserve University, Cleveland, OH, USA.

Abstract

Alzheimer's disease (AD) is the leading cause of dementia in the elderly, characterized clinically by progressive decline in cognitive function and neuropathologically by the presence of senile plaques and neuronal loss in the brain. While current drugs for AD are always employed as symptomatic therapies with variable benefits, there is no treatment to delay its progression or halt neurodegeneration. TAR DNA-binding protein 43 (TDP-43) proteinopathy has increasingly been implicated as a prominent histopathological feature of AD and related dementias. Our recent studies have implicated mitochondria as critical targets of TDP-43 neurotoxicity. Here, we demonstrate that the suppression of mitochondrial-associated TDP-43 protects against neuronal loss and behavioral deficits in 5XFAD transgenic mice recapitulating AD-related phenotypes. In AD patients and 5XFAD mice, the level of TDP-43 is increased in mitochondria, and TDP-43 highly co-localizes with mitochondria in brain neurons exhibiting TDP-43 proteinopathy. Chronic administration of a TDP-43 mitochondrial localization inhibitory peptide, PM1, significantly alleviates TDP-43 proteinopathy, mitochondrial abnormalities, microgliosis and even neuronal loss without effect on amyloid plaque load in 12-month-old 5XFAD mice well after the onset of symptoms. Additionally, PM1 also improves the cognitive and motor function in 12-month-old 5XFAD mice and completely prevents the onset of mild cognitive impairment in 6-month-old 5XFAD mice. These data indicate that mitochondria-associated TDP-43 is likely involved in AD pathogenesis and that the inhibitor of mitochondria-associated TDP-43 may be a valuable drug to treat underlying AD.

*Correspondence to: Xinglong Wang (xinglong.wang@case.edu).

[1]These authors contributed equally to this work

Abstract

One Sentence Summary: Targeting mitochondrial-associated TDP-43 for the treatment of Alzheimer's disease.

Keywords

TDP-43; amyloid beta; Alzheimer’s disease; mitochondrial dysfunction; neurodegeneration; memory loss

1. Introduction

Alzheimer's disease (AD) is the most prevalent form of dementia in the elderly, characterized by the progressive loss of neurons in brain regions critical for memory and cognition, along with the pathologic hallmarks, senile plaques (SPs) and neurofibrillary tangles (NFTs), in which amyloid-β peptide (Aβ) and tau are the main components, respectively [1]. Currently, there is no effective treatment for AD. Genetic mutations in TAR DNA-binding protein 43 (TDP-43) cause amyotrophic lateral sclerosis (ALS) and frontotemporal dementia (FTD), which is the second most common form of early-onset dementia [2-4]. TDP-43 proteinopathy, usually referred to as cytoplasmic TDP-43 accumulation, is a prominent histopathological feature of degenerating neurons in patients with ALS or FTD [5, 6]. In fact, increasing evidence indicates that TDP-43 proteinopathy may represent a key pathological feature in common dementias, including the clinical syndrome of AD and related dementia syndromes [7-13]. In AD patients, TDP-43 pathology originates from the amygdala spreading to memory-controlling areas of the cortex (medial temporal lobe and subsequent neocortex), demonstrating a very distinct pathway, which is different from the routes taken by SP or NFT progression [11, 14]. More importantly, TDP-43 proteinopathy is associated with AD-type dementia independent of NFTs and SPs, and patients with mixed TDP-43, Aβ, and tau proteinopathies show more severe AD-type dementia than patients with Aβ and tau proteinopathies alone [8, 15]. Despite an expanding body of evidence implicating the important role of TDP-43 in AD and related dementia, the role of TDP-43 proteinopathy in disease progression is largely unknown and little attempt has been taken to investigate the possibility of targeting TDP-43 for the treatment of these devastating diseases.

Previous studies have repeatedly showed abnormal mitochondrial morphology [16-18], transport [17, 18], even function [17, 19, 20] in cells or mice expressing either wild type or mutant TDP-43, indicating mitochondria as likely targets of TDP-43. This notion is further supported by evidence showing that TDP-43 or truncated forms of TDP-43 can be present in either the inside or outside of mitochondria [21-27]. Among these studies, most recent study and we have independently found that the portion of full-length TDP-43 inside of mitochondria can bind mitochondria-transcripted messenger RNA (mRNAs) encoding subunits (ND3/6) of oxidative phosphorylation (OXPHOS) complex I to specifically impair its assembly and function [21, 27], whereas truncated TDP-43 lacking the M1 mitochondrial localization sequence [27] is restricted to the inner membrane space and has no effect on ND3/6 expression or mitochondrial function [21]. We have shown that TDP-43 accumulates

in mitochondria in ALS and FTD patients, and that the suppression of TDP-43 mitochondrial localization can prevent neuronal death and behavioral deficits in TDP-43 transgenic mice for ALS and FTD [27, 28], defining mitochondria as a critical mediator for TDP-43 neurotoxicity in diseases. So far, there is few study of TDP-43 in mitochondria in AD. Here, we examined the localization and expression of TDP-43 in degenerating neurons in AD patients and 5XFAD transgenic mice recapitulating AD-related phenotypes [29, 30]. To investigate the contribution of mitochondria-associated TDP-43 to AD progression, we further studied the therapeutic effects of a TDP-43 mitochondrial localization inhibitory peptide on mitochondria, neurodegeneration, and cognitive function in both aged and young 5XFAD mice.

2. Materials and methods

2.1. Animals and treatments

Mouse surgery and procedures were performed according to NIH guidelines and were approved by the Institutional Animal Care and Use Committee (IACUC) at Case Western Reserve University.

All aged NTG and 5XFAD female mice (B6SJL-Tg (APPSwFlLon, PSEN1*M146L*L286V) 6799Vas/Mmjax, stock no. 34840-JAX) used in behavioral tests were born at the same day, directly purchased from the Mutant Mouse Resource & Research Centers (MMRRC) and maintained at Case Western Reserve University. The cohort of young NTG and 5XFAD mice was generated and maintained at Case Western Reserve University, weaned on postnatal day 30 and genotyped by PCR analysis of DNA extracted from an ear punch. Detailed mouse age and gender information for each experiment is presented in specific figure legends. cPM and PM1 peptides fused to the C terminus of the protein transduction domain (YGRKKRRQRRR) of the human immunodeficiency virus TAT protein to enhance peptide delivery and permeability as described [27, 31] were obtained from Biomatik (Wilmington, DE). For peptide infusion, mini osmotic pumps (Alzet model 1004, flow rate of 0.11 μL/hr) were filled with 100 μL PBS containing cPM or PM1 peptides (0.5 mg/kg/day) followed by pump incubation in PBS at 37°C overnight according to the manufacturer’s instructions. After isoflurane anesthesia, mini osmotic pumps were implanted subcutaneously in the back of each mouse. After treatment, mice were transcardially perfused with ice cold PBS and brain tissues were collected.

2.2. Behavioral tests

All mice were subjected to a battery of behavioral assessments including motor tasks (open field test), body coordination tasks (rotarod and footprint test), muscle strength (grip strength test) and cognitive tasks (Barnes maze test for long-term spatial memory). To avoid habituation, individual mice were tested for these behavioral tasks on each test day in the following order: day 1-4 for rotarod and grip strength test, day 5 for open field test and day 6-10 for Barnes maze test. All tests were performed at the Case Behavior Core, with the investigator blinded to both mouse genotype and treatment group. Before the rotarod testing, mice received 3 training trials per day for 3 days by placing them on the Rota-Rod (Panlab/Harvard Apparatus, Holliston, MA) with gradually increased cylinder speeds from 4 rpm to

12 rpm. On the testing day, the maximal latency to fall off was recorded in the rotarod set to the accelerating mode (speed increasing from 4 to 40 rpm in 5 minutes). For the muscular strength measurement, the two forepaws of a mouse were placed on a grid with the two hindpaws placed on a bar that was connected to a grip strength test meter (Bioseb, Vitrolles, France) for 5 trials. The single best recorded value was collected for statistical analysis. The open field test used a 50cm long square plastic apparatus closed with 50cm high walls with the activity recorded continually for 10 minutes by ANY-maze video tracking software (Stoelting Co. Wood Dale, IL). The footprint tests were performed using a customized runway with 50 cm long, 5 cm wide and both sides bordered as we described [27].

The Barnes maze consisted of a white acrylic circular disk 92 cm in diameter with 20 equally spaced holes (5cm in diameter) located 2 cm from the edge of the disk. The maze was illuminated by two 60W lamps to provide an aversive, bright disk surface. An acrylic escape box (7 × 7 × 5 cm) could be fitted under any of the holes in the maze. The maze was raised 30 cm from the floor and rested on a pedestal that enabled it to be rotated 360° on a horizontal plane. An acrylic start bin with 15 cm diameter and 15 cm height was used. Trials were recorded using a webcam and analyzed by video tracking software (EthoVision XT, Noldus, Leesburg, VA). Each trial began with the start bin positioned in the center of the maze with the mouse placed inside. The mouse remained in the start bin for 30 seconds, providing a standard starting context for each trial and ensuring that initial orientation of the mouse in the maze varied randomly from trial to trial. Each mouse was allowed to explore the maze freely for 2 minutes. After the mouse entered the escape hole, the mouse was left in the escape box for 90 seconds before being returned to its home cage. If the mouse did not enter the escape box within 120 seconds, it was gently picked up by the experimenter and placed over the target hole and allowed to enter the escape box. After each trial, the maze and escape box were cleaned carefully with a 10% alcohol solution to dissipate odor cues and provide a standard olfactory context. Five training sessions consisting of two trials each were run on subsequent days and escape latencies were measured.

2.3. Mitochondrial isolation

Brain tissues were homogenized in IB-1 solution (225 mM mannitol, 75 mM sucrose, 0.5 mM EGTA, and 30 mM Tris-HCl [pH 7.4]), followed by centrifugation at 600 g for 5 min to remove nuclear contaminants and unbroken cells. The supernatant was further centrifuged at 600 g for 5 min and at 9,000 g for 10 min. The pellet was then washed two times in IB-2 solution (225 mM mannitol, 75 mM sucrose, and 30 mM Tris-HCl [pH 7.4]) and resuspended in mitochondria resuspending buffer (MRB) (250 mM mannitol, 5 mM HEPES [pH 7.4], and 0.5 mM EGTA). The resuspended fraction was overlaid on top of 4 mL Percoll medium (225 mM mannitol, 25 mM HEPES [pH 7.4], 1 mM EGTA, and 30% Percoll [v/v]) and centrifuged at 95,000 g in a SW50.1 rotor for 30 minutes at 4°C. The purified mitochondrial fraction was collected and resuspended in a 10-fold volume of MRB and centrifuged for 10 min at 6,300 g to obtain purified mitochondria.

2.4. Immunoblot, immunocytochemistry, and immunofluorescence

The use of all human tissue samples was approved by the University Hospitals Institutional Review Board (IRB) for human investigation at the University Hospitals Case Medical

Center in Cleveland, Ohio. Brain tissues or purified mitochondria were homogenized or lysed in cell lysis buffer (20 mM Tris-HCl (pH 7.5), 150 mM NaCl, 1 mM Na_2EDTA, 1 mM EGTA, 1% Triton, 2.5 mM sodium pyrophosphate, 1 mM b-glycerophosphate, 1 mM Na_3VO_4, 1 μg/ml leupeptin; Cell signaling, Danvers, MA) with 1×protease inhibitor cocktail (Sigma-Aldrich, St. Louis, MO). Proteins were separated by 10% SDS-PAGE and transferred to a polyvinylidene fluoride (PVDF) membrane. Following incubation with primary antibody overnight in 4°C and secondary antibodies at room temperature (RT) for 1 hour, immunoreactivity was detected by enhanced chemiluminescence (ECL) (Millipore Immobilon). Primary antibodies used in this study are listed in table S1.

Postmortem human tissues obtained from University Hospitals of Cleveland were fixed and 6-μm-thick consecutive sections were prepared as we described before [27] (table S2). Immunocytochemistry was performed by the peroxidase anti-peroxidase protocol [32]. Taken briefly, paraffin embedded brain tissue sections were first deparaffinized in xylene and rehydrated in graded ethanol and incubated in Tris Buffered Saline (TBS, 50 mM Tris·HCl and 150 mM NaCl, pH = 7.6) for 10 minutes before performing antigen retrieval in 1X antigen decloaker (Biocare) as described previously [27]. Sections were rinsed with distilled H_2O, incubated in TBS for 10 minutes and blocked with 10% normal goat serum (NGS) in TBS at RT for 30 minutes. Tissue sections were further incubated with primary antibodies in TBS containing 1% NGS overnight at 4°C and immunostained by the peroxidase-anti-peroxidase based method as we described [33]. For immunofluorescence staining, deparaffinized and rehydrated tissue sections were washed briefly three times with distilled H_2O and antigen retrieval was performed as before [27]. The sections were then blocked with 10% NGS for 30 minutes at RT and incubated with primary antibodies in PBS containing 1% NGS overnight at 4°C. After three washes with PBS, the sections were incubated in 10% NGS for 10 minutes and then with Alexa Fluor conjugated secondary antibody (Life Technologies, Grand Island, NY) (1:300) for 2 hours at RT in the dark. Finally, the sections were rinsed three times with PBS, stained with DAPI for nuclei, washed again with PBS three times, and mounted with Fluoromount-G mounting medium (Southern Biotech, Birmingham, AL). All sections were blindly examined by two investigators independently.

2.5. Confocal microscopy, fluorescent microscopy and electron microscopy

Confocal images were captured at RT with a Leica TCS SP8 STED inverted laser-scanning confocal fluorescence microscope (controlled through LAS X software, Leica). Fluorescent images from whole brain sections were captured with a Zeiss automated microscope, Celldiscoverer 7 (controlled by Zen software, Zeiss). Whole brain slides were scanned with a 20x(0.75) PIan Apochromat dry objective. To visualize TDP-43 mislocalization in 5XFAD mice, images were captured with a 100x water objective, a standard Z-stack scans were performed and deconvolution conducted with Zen software.

For regular EM, samples were freshly dissected and processed as previously described [34]. Small pieces of cortical tissue or isolated mitochondria were fixed by immersion in triple aldehyde–DMSO. After rinsing in distilled water, they were postfixed in ferrocyanide-reduced osmium tetroxide. Another water rinse was followed by an overnight soak in

acidified uranyl acetate. After rinsing in distilled water again, the tissue blocks were dehydrated in ascending concentrations of ethanol, passed through propylene oxide, and embedded in Poly-Bed resin. Thin sections were sequentially stained with acidified uranyl acetate followed by a modification of Sato's triple lead stain and examined in an FEI Tecnai Spirit (T12) with a Gatan US4000 4kx4k CCD.

For immuno-EM, human brain tissue and isolated mitochondria were fixed in 4% w/v formaldehyde containing 0.1% w/v glutaraldehyde in 0.1 M HEPES buffer (Electron Microscopy Sciences, Hatfield, PA) at RT for 45 minutes, then dehydrated in ethanol and embedded in LR White resin (Polysciences, Inc., Warrington, PA). Immuno-gold labeling was performed according to the method described by Fujioka et al [35]. Thin sections were blocked with PBS containing 1% w/v bovine serum albumin (BSA), 1% v/v normal goat serum and 0.01% v/v Tween 20 (PBGT). Grids were then incubated with antibodies (6E10 and anti-TDP-43) at 1:10–1:30 dilution in PBGT for 12 h at 4 °C. Negative controls included normal rabbit serum, normal mouse serum, and PBT replaced as the primary antibody. After washing, grids were incubated for 1.5 hour in 10nm gold-conjugated goat anti-rabbit IgG or goat anti-mouse IgG (British BioCell International, Ted Pella, Inc., Redding, CA) diluted 1:20 in PBGT, rinsed with PBS and fixed with glutaraldehyde to stabilize the gold particles. Gold-labeled thin sections were stained first with 2% acidified uranyl acetate at 38 °C for 30 minutes, then with the triple lead stain of Sato as modified by Hanaichi et al [34], then examined in an FEI Tecnai Spirit (T12) with a Gatan US4000 4kx4k CCD. All sections were blindly examined by two investigators independently.

2.6. Thioflavin-S staining and plaque quantification

Paraffin embedded brain tissue sections were deparaffinized and rehydrated before being processed for Thioflavin-S (Thio-S) staining as described by Schmidt and collaborators [36]. Briefly, sections on slides were incubated in filtered 1% aqueous Thioflavin-S for 8 minutes at room temperature and were protected from light, then washed with 80% ethanol twice and 95% ethanol once. After three washes with distilled water, slides were coverslipped using mounting media and allowed to dry in the dark overnight. Whole brain images of 5XFAD mice treated by PM1 or cPM stained with Thio-S were scanned using the Celldiscoverer 7 with a 20x (0.75) PIan Apochromat dry objective. The color images for plaques were converted to binary images. Plaque numbers and average size were counted automatically by Image-Pro Plus 6.0 software after setting the brightness threshold. Plaque load was defined as total plaque area/special brain area. All sections were blindly analyzed and quantified by two investigators independently.

2.7. Neuron, microglia, and astrocyte quantification

Digitized images, acquired keeping all the parameters (contrast and brightness) constant, were transformed into TIFF files and thresholded using Image Pro Plus 6.0 software. Care was taken to maintain the same threshold in all sections from the same experiment. Neuronal cell number counts of NeuN positive cells in the cortices and subicula were automatically performed using Image Pro Plus 6.0 software, and cell numbers were calculated per mm^2. In the hippocampi, cell numbers were manually counted because of neuron density. Microglia and astrocytes were counted manually after setting the brightness threshold. Quantitative

comparisons were carried out blindly on sections processed at the same time with the same batch of solutions. All number/mm^2 data were finally normalized to cPM treated group. Detailed mouse age and gender information for each experiment is presented in specific figure legends.

2.8. Blue-native PAGE and In-gel Enzyme Activity Assay of Mitochondrial Complex I

Blue-native gel electrophoresis of mitochondrial OXPHOS complexes was performed with NativePAGE Bis-Tris Gel system (Life Technologies, Grand Island, NY). 50 μg isolated mitochondria were resuspended in sample buffer and solubilized with 2% digitonin (Sigma-Aldrich) for 30 min on ice. Insolubilized pellets were removed by centrifugation for 30 min at 14,000g. The supernatant was collected, and 5% G-250 sample additive was added. Samples were loaded to 3–12% precast Bis-Tris gradient gels (Life Technologies, Grand Island, NY), followed by electrophoresis with manufacturer's instructions. The gel strip was incubated in 20 ml of 20 mM Tris-HCl buffer (pH 7.4) containing 0.2 mg/ml NBT and 0.1 mg/ml NADH, and then developed within 20 min at room temperature. The reactions were stopped by fixing the gel for 30 min in a solution containing 50% methanol (v/v) and 10% acetic acid (v/v).

2.9. Dot Blot

Brain tissues or purified mitochondria were homogenized or lysed in cell lysis buffer with 1×protease inhibitor cocktail (Sigma-Aldrich, St. Louis, MO). Protein concentrations of the supernatant were measured using a BCA assay and 20 μg of extract was applied to a nitrocellulose membrane using the Bio-Dot microfiltration apparatus (Bio-rad, Hercules, CA) following manufacturer's instructions. After being incubated with 6E10 and HRP-conjugated secondary antibody, the membrane was visualized using ECL. Aβ levels were quantified using Image J Software.

2.10. Statistical Analysis

Statistical analyses were performed with Student's *t*-test, one-way analysis of variance (ANOVA) and two-way ANOVA. Detailed information about statistical analysis for each experiment is presented in specific figure legends. Data are means ± s.e.m. n represents number of neurons or mice per experiment. $P < 0.05$ was considered to be statistically significant.

3. Results

3.1. TDP-43 is augmented in the mitochondria of AD patients and 5XFAD transgenic mice

We first investigated the colocalization of TDP-43 with mitochondria in neurons of human cortex tissue from AD cases and age-matched normal individuals by double immunofluorescence staining using antibodies specific to TDP-43 and outer mitochondrial membrane marker Tom20. Cortical neurons in control cases demonstrated mainly nuclear TDP-43 localization, yet cortical neurons in the AD cases showed characteristic increased cytoplasmic TDP-43 (Fig. 1A). Notably, cytoplasmic TDP-43 in AD cortical neurons significantly colocalized with mitochondria (Fig. 1A). Immuno-electron microscopy (immuno-EM) analysis of isolated highly purified mitochondria with well-preserved

membranes from human cortical tissues showed TDP-43 predominantly in the inner mitochondrial membrane cristae not overlapping with Aβ labeling in all AD and control samples (Fig. 1A and Supplementary Fig. 1A, B). Mitochondria from AD cortices demonstrated greater TDP-43 labeling than those from age-matched controls (Fig. 1B). Consistently, immunoblot analysis revealed that there was indeed a significantly higher expression of TDP-43 in purified mitochondria from AD than age-matched controls, while the levels of TDP-43 in total tissue lysate remained unchanged (Fig. 1C). Significant cytoplasmic TDP-43 accumulation could be noted selectively in neurons of the subiculum and cortex but not in the hippocampus CA1 of 9-month-old 5XFAD mice (Supplementary Fig. 1C), a widely used APP/PS1 transgenic mouse model for AD that demonstrate robust neurodegeneration and cognitive deficits [29, 30]. Similar to the findings in AD patients, cytoplasmic TDP-43 highly colocalized with mitochondria in neurons of 5XFAD mice (Fig. 1D and Supplementary Fig. 1D). Whereas all mice displayed comparable expression of total TDP-43, 5XFAD mice demonstrated significantly higher levels of TDP-43 in purified mitochondria than age-matched non-transgenic (NTG) littermates (Fig. 1E). As another feature of TDP-43 proteinopathy, phosphorylated TDP-43 positive inclusions could be observed in the cytoplasm of both AD patient and 5XFAD mouse, and found greatly colocalized with mitochondria (Fig. 1F and Supplementary Fig. 1E,F).

3.2. Alleviation of TDP-43 proteinopathy and mitochondrial abnormalities in aged 5XFAD mice by inhibition of TDP-43 mitochondrial localization

TDP-43 mitochondrial localization depends on its M1 motif, the deletion of which suppresses its mitochondrial accumulation without significant effect on its half-life, dimerization, functional binding to mRNA targets, and expression of cytosolic, nuclear, or total TDP-43 [27]. The synthesized peptide PM1 (*YGRKKRRQRRRAQFPGACGL*) in which the M1 motif was fused to the TAT peptide (*GRKKRRQRRR*), competitively inhibits TDP-43 mitochondrial localization and abolishes TDP-43-induced toxicity on mitochondria and neurons without affecting on total or nuclear TDP-43 expression [27]. We next determined whether increased expression of TDP-43 in mitochondria in aged 5XFAD mice after the appearance of TDP-43 proteinopathy and neuronal loss could be reversed by PM1. 10 months old 5XFAD transgenic mice were subcutaneously infused with either PM1 or control cPM peptide at a dose of 0.5 mg/kg/day continuously for 4 weeks followed by a 2-week washout period to eliminate the potential effect of the treatment (Fig. 2A). We confirmed that PM1, as indicated by TAT staining, reached the central nervous system (Supplementary Fig. 2A) and greatly reduced the levels of mitochondrial TDP-43 in the brains of 12-month-old 5XFAD mice (Fig. 2B). After PM1 peptide infusion, TDP-43 cytoplasmic accumulation in the subiculum was significantly reduced and TDP-43 was predominantly restricted to the nucleus (Supplementary Fig. 2B,C). In addition, phosphorylated TDP-43 positive inclusions were rarely seen in aged 5XFAD mice with PM1 infusion (data now shown), together suggesting that the suppression of TDP-43 mitochondrial localization is sufficient to reverse TDP-43 proteinopathy in 5XFAD mice.

Within mitochondria, TDP-43 binds mitochondria-transcribed mRNAs encoding oxidative phosphorylation (OXPHOS) complex 1 key subunits, ND3 and ND6, and specifically impairs their function [27]. ND3 protein level in 5XFAD mice was significantly increased by

PM1 infusion, compared with cPM (Fig. 2C). There was also a trend of increased levels of ND6 in PM1 treated mice without affecting any other OXPHOS complex components (Fig. 2C and Supplementary Fig. 2D). Consistent with the protective effect against the reduction in mitochondrial complex I subunits, PM1 infusion improved both assembly and activity of mitochondrial complex 1 in 12-month-old 5XFAD mice (Fig. 2D,E). Although PM1 peptide had no effect on the expression of mitochondrial dynamic regulators such as Drp1, Mff, OPA1, and Mfn2 (Supplementary Fig. 2E), abnormal dumbbell-shaped mitochondria in the cortical neurons of 12-month-old 5XFAD mice were largely absent after PM1 treatment (Fig. 2F), indicating the inhibition of TDP-43 mitochondrial localization can prevent mitochondrial abnormalities.

3.3. Unchanged Aβ plaque deposition in aged 5XFAD mice following PM1 administration

To determine whether alleviated TDP-43 proteinopathy and mitochondrial abnormalities in aged 5XFAD mice were due to decreased Aβ, we first examined the impact of PM1 on Aβ plaque deposition by Thioflavin-S (Thio-S) staining. Although the plaque size was very similar in the subiculum, cortex, or hippocampus, the plaque load, expressed as the percentage of total surface of brain tissue covered by Aβ plaques, was particularly high in the subiculum (Fig. 3A). No significant change in the numbers, size, and load of Thio-S-positive plaques was noted in 12-month-old 5XFAD mice after PM1 infusion (Fig. 3A), suggesting that the inhibition of TDP-43 mitochondrial localization has no effect on fibrillary dense-core plaques. It has been established that Aβ exists as a monomer, and also as oligomers, protofibrils, and fibrils [37]. Aβ oligomers are considered to be more toxic than fibrillar Aβ or SPs [37, 38]. To examine if the alleviated TDP-43 proteinopathy by PM1 was associated with reduced oligomer Aβ, we conducted immunostaining using the oligomer Aβ specific antibody NU4 as described [39]. Compared to Thio-S, NU4 stained less Aβ plaques with markedly decreased size in the subiculum (Fig. 3B). Additionally, in the cortex and hippocampus, there were more diffusive plaques stained by NU4. Like Thio-S-positive plaques, the density, size and number of NU4-positive plaques in all brain areas of PM1-treated 12-month-old 5XFAD mice were comparable to cPM-treated littermates (Fig. 3B). These data are in agreement with the similar plaque deposition or intraneuronal APP/Aβ immunoreactivity in all animals stained by 6E10, which recognizes both APP and its cleavage products (Supplementary Fig. 3A). Further dot blot examination revealed that the total amount of Aβ remained unchanged in total brain homogenates and purified mitochondria after PM1 infusion (Supplementary Fig. 3B). Taken together, these results indicate that the suppression of TDP-43 mitochondrial localization by PM1 does not affect Aβ plaque deposition.

3.4. Protection against neuron loss and gliosis in the subiculum of aged 5XFAD mice via PM1

Since neuronal cell numbers significantly decreased in the subicula and cortical layer 5 of aged 5XFAD mice, we next determined the effects of PM1 on subiculum neurons in 12-month-old 5XFAD mice. After PM1 treatment, neuronal cell numbers in the subicula and cortical layer V of 12-month-old 5XFAD mice were significantly increased by either NeuN or Nissl staining when compared to cPM treatment (Fig. 4A and Supplementary Fig. 4A). Neuroinflammation is a prominent pathological feature of AD characterized by the

proliferation and activation of microglia and astrocytes (i.e., microgliosis and astrogliosis), which have been reported in 5XFAD mice [40, 41]. To examine the extent of microgliosis and astrogliosis in aged 5XFAD mice following PM1 administration, we immunostained activated microglia and astrocytes in the brain of 12-month-old mice with specific antibodies against ionizing calcium binding adaptor molecule 1 (Iba1) and glial fibrillary acidic protein (GFAP) respectively. Likely corresponding to high Aβ plaque deposition and neuronal loss in the subiculum, aged 5XFAD mice exhibited the predominance of microgliosis and astrogliosis in this specific brain area (Fig. 4B and Supplementary Fig. 4B). Interestingly, quantification revealed significantly reduced microgliosis but not astrogliosis in all the selected brain areas of 12-month-old mice treated by PM1 (Fig. 4B and Supplementary Fig. 4B), suggesting the specific inhibition of microgliosis by suppressing TDP-43 mitochondrial localization.

3.5. Improved cognitive and motor function in aged 5XFAD mice following PM1 administration

Although 5XFAD mice are viable and phenotypically normal at birth, they begin to show cognitive deficits at around 4 months old and motor-coordinative deficits at around 5 months old (Fig. 2A) [42, 43]. We conducted a series of behavioral tests to investigate the cognitive and motor performances in 12-month-old 5XFAD mice after PM1 treatment. Although 5XFAD mice showed significantly decrease in body weight at 12-month-old compared with NTG, no differences in brain weight, and skeletal muscle mass were noted in 5XFAD mice infused with cPM or PM1 (Fig. 5A,B and Supplementary Fig. 5A). PM1-treated aged 5XFAD mice showed similar traveling distance and moving speed in open field tests with both cPM and NTG mice, indicating that the locomotor activity and anxiety-related behavior were not altered by peptide treatment (Fig. 5C,D). A Barnes maze task consisting of 5 blocks was further used to assess the cognitive benefits of PM1. Unlike NTG mice showing a decreased time to enter the escape hole in Block 3 and thereafter compared to Block 1, cPM-treated 5XFAD mice barely exhibited any difference in time for escape in all trials (Fig. 5E), indicating severely impaired performance over the trials. After PM1 treatment, 5XFAD mice displayed significantly improved ability to find the escape hole in block 4 and 5 (Fig. 5E), suggesting that the suppression of TDP-43 mitochondrial localization by PM1 enhanced spatial learning of 5XFAD mice. To further test spatial working memory of aged 5XFAD mice, we conducted a Y maze test. Aged 5XFAD mice showed a significantly lower ratio of spontaneous alternations than NTG mice, suggesting impaired spatial working memory. Although there was no significant difference, PM1 treatment showed a trend of improved in spatial working memory (Fig. 5F). Then we assessed the motor and coordination function of 5XFAD mice by rotarod test before and after treatment. We confirmed that there was no significant difference in rotarod performance between cohorts of 10-month-old 5XFAD mice for PM1 and cPM infusion before treatment (Supplementary Fig. 5B). However, compared with mice treated with cPM, 5XFAD mice with PM1 infusion exhibited a trend of improved motor coordination and balance (Fig. 5G). Consistently, despite unchanged muscle strength, walking abnormality (decreased stride length) was significantly alleviated in aged 5XFAD mice after PM1 treatment as indicated by footprint test (Fig. 5H and Supplementary Fig. 5C).

3.6. Prevention of cognitive deficits in young 5XFAD mice by PM1

Considering the significant protective effects of PM1 in aged 5XFAD mice, we also investigated whether PM1 was sufficient to prevent the onset of cognitive impairment observed in young 5XFAD mice. 3-month-old 5XFAD mice were continuously infused with either PM1 or control cPM peptide and then a series of behavioral tests were performed after 10 weeks (Fig. 6A). Similar with aged 5XFAD mice, both cPM and PM1-treated 5-month-old 5XFAD mice showed similar traveling distance and moving speed in open field tests (Supplementary Fig. 6A,B). Further Barnes maze test were conducted to investigate the cognitive performance. Although all 6-month-old mice actively explored the maze and showed reduced escaping time over trials, 5XFAD mice infused with cPM spent significantly more time finding the escape hole (Fig. 6B). In contrast, young 5XFAD mice treated with PM1 demonstrated similar performance in all trials compared to age-matched NTG littermates, therefore suggesting that the inhibition of TDP-43 mitochondrial localization by PM1 could abolish the decline in spatial learning in young 5XFAD mice. Although all 5XFAD mice displayed deficits on the rotarod test at 5 months old compared with NTG littermates, 5XFAD mice treated by PM1 also showed a trend of improved motor coordination and balance (Supplementary Fig. 6C). In 5XFAD mice, Aβ plaques first appear at 2-3 months old and rapidly increases at around 4 months old [41]. Aβ plaque load measured by Thio-S staining was not significantly different between cPM-treated young 5XFAD mice versus aged-matched 5XFAD littermates treated with PM1 (Fig. 6C). Similar with aged 5XFAD mice, PM1 could also alleviate microgliosis at 6-month-old compared to cPM treatment group (Fig. 6D). These findings consistently indicate that the suppression of TDP-43 mitochondrial localization by PM1 could alleviate Aβ toxicity *in vivo*.

4. Discussion

Here, our study demonstrates that a peptide inhibitor of mitochondrial TDP-43 administered late in the course of disease can attenuate the development and progression of brain neuronal loss and behavioral deficits in the 5XFAD transgenic mouse model for AD. Our previous study has reported a similar striking rescue effects on brain neurons and cognitive performance by the suppression of TDP-43 mitochondrial localization in the advanced-stage of a TDP-43 transgenic mouse model demonstrating FTD-like dementia [28]. Similar to FTD patients [27], AD patients show significantly increased expression of TDP-43 in mitochondria. Therefore, our findings suggest that TDP-43 accumulation in mitochondria is likely a common mechanism underlying neurodegeneration and cognitive decline in AD and other dementia syndrome, and that an inhibitor of TDP-43 mitochondrial localization may provide a potential AD drug to treat the underlying disease or delay its progression.

The accumulation of TDP-43 in the cytoplasm or phosphorylated TDP-43 positive inclusion was largely noted in subicular neurons of 5XFAD mice, correlating with the most significant neuronal loss and amyloid plaque load in this restricted area. Mislocalized TDP-43 highly colocalizes within mitochondria. We used PM1, a peptide inhibitor derived from TDP-43, to specifically reduce its expression in mitochondria. PM1 abolished TDP-43 proteinopathy, reversed neuronal loss, and reduced neuroinflammation in aged 5XFAD mice well after symptom onset. As amyloid plaque load was not alleviated or prevented by PM1, our results

strongly indicate that TDP-43 in mitochondria does not affect Aβ pathology, but instead plays an unexpected critical role in mediating Aβ neurotoxicity. Brains of 5XFAD mice exhibited reduced expression of ND3/6, deficiency in mitochondrial complex I activity, and abnormal mitochondrial morphology, all of which were significantly alleviated by PM1. Within mitochondria, TDP-43 binds mitochondria-transcribed ND3/6, impairs their translation and causes mitochondrial dysfunction [27]. Thus, although it is underdetermined why TDP-43 mislocalizes particularly in subiculum neurons and how mitochondrial-associated TDP-43 acts on mitochondria in the context of Aβ, this evidence supports the possible involvement of mitochondrial TDP-43-related mitochondrial dysfunction in the neuronal loss of 5XFAD mice.

5XFAD mice demonstrated significant impairment in spatial learning and memory. Interestingly, the subiculum is a component of hippocampus and plays a crucial role in spatial learning and memory functions [44]. Consistent with the rescue of subiculum neurons, spatial learning and memory was significantly improved by PM1, indicating that the cognitive deficit in 5XFAD mice was likely caused by neuronal loss in the subiculum. In addition to the subiculum, neuronal loss can also be seen selectively in cortical layer 5 but not in the hippocampus of 5XFAD mice. Although neuronal loss was modest in cortical layer 5 and only a few cortical neurons displayed mild TDP-43 proteinopathy, PM1 treatment restore the neuron number of aged 5XFAD mice to the NTG level in this area. Considering the two-week washout period added in this study, long-term or continuous PM1 administration may be necessary for neurogenesis to replenish subiculum neurons to NTG level. It is conceivable that PM1 could restore subiculum and cortical neurons in 5XFAD mice via neurogenesis. PM1 alone does not induce neurogenesis in NTG mice, excluding the possibility of over-neurogenesis. Although the prevention of TDP-43 proteinopathy in subiculum neurons by PM1 strongly indicates neuroprotective effect, neurogenesis may be impaired in the subiculum of 5XFAD mice and future studies are needed to clarify the effect of PM1 on the generation of subiculum neurons from neural stem cells. Although TDP-43 proteinopathy has been reported in neuroinflammatory cells [45], astrocytic or glial TDP-43 pathology was not noted in 5XFAD mice, and PM1 administration in NTG showed no effect on the basal level of astrocyte and microglia activation, suggesting that PM1 unlikely primarily acts through the neuroinflammatory mechanism (s).

In addition to mitochondria, TDP-43 could be present in different subcellular organelles. Also, despite its likely primary function in RNA processing, TDP-43 exhibits diverse roles in regulating autophagy [46, 47], cell cycle [48, 49], endosomal trafficking [50], mitochondrial bioenergetics [25, 27] and fat metabolism [51]. Although this study could not exclude the possibility that TDP-43 may contribute to neuronal loss and cognitive impairment indirectly from its cytosolic or nuclear localization in 5XFAD mice, nuclear TDP-43 remained unchanged in 5XFAD mice and cytoplasmic TDP-43 accumulation could be blocked by the suppression of TDP-43 mitochondrial localization, indicating a critical role of mitochondrial TDP-43 in mediating Aβ-induced TDP-43 proteinopathy. It is still unclear how PM1 decreased cytosolic localization of TDP-43. Although no study shows the proteasome-dependent degradation of matrix facing inner mitochondrial membrane (IMM) proteins, both the ubiquitin proteasome system (UPS) and autophagy pathways have been implicated in cytosolic TDP-43 clearance [52, 53]. Therefore, it is possible that the reduced

cytosolic TDP-43 by TDP-43 mitochondrial localization suppression is due to activated UPS or autophagy. The interplay between mitochondrial TDP-43 and the protein quality control system in AD needs further detailed investigation.

Unlike TDP-43 in ALS or FTD mitochondria [27], TDP-43 in AD mitochondria tends to form “clusters” in cristae. Aβ and TDP-43 did not co-localize in mitochondria by immuno-EM (Supplementary Fig. 1B). Therefore, it is unlikely that Aβ regulates TDP-43 mitochondrial localization through direct interaction. The expression of total TDP-43 remains unchanged in AD patients and 5XFAD mice, indicating unlikely no alterations of global protein translation or turnover of TDP-43. As there is no export pathway(s) for proteins localized in mitochondria, the increased mitochondrial TDP-43 in AD or 5XFAD mice should be caused by increased import, impaired clearance or both. There are more than 10 putative proteases (mitoproteases) located in the matrix of mammalian mitochondria. LONP1 has been reported as a mitoprotease degrading TDP-43 within mitochondria [54, 55]. Mitoprotease PreP has been implicated in Aβ clearance within mitochondria [56], which may also indirectly regulate mitochondrial TDP-43 degradation. Additionally, like many mitochondrial proteins [57], the import of TDP-43 depends on mitochondrial membrane potential (mΔψ) [27]. Although our previous studies showed that mΔψ was reduced by Aβ, the detailed mechanisms by which TDP-43 is imported across mitochondrial outer and inner membrane remain largely unknown [58, 59]. The partial reduction of mΔψ by Aβ might affect, but is unlikely completely to abolish TDP-43 import in the context of Aβ. Considering that molecular chaperones are usually needed to unfold protein before and during import [60], it could be anticipated that the degradation of mitochondrial TDP-43 or the import of TDP-43 into mitochondria should depend on multiple factors including, but not limited to, LONP1, PreP, mΔψ and chaperones. Although it is unlikely that LONP1 or other factors regulate mitochondrial function specifically through mitochondrial TDP-43, future studies will be needed to test the necessity and sufficiency of LONP1 or these factors for mitochondrial TDP-43 clearance in AD.

The most recent study and we independently reported the presence of full-length TDP-43 inside of mitochondria using biochemical, genetic and immunostaining approaches [21, 27]. In this study, by immuno-EM, we consistently demonstrated strong TDP-43 immunoreactivity inside of mitochondria largely associated with cristae. Unlike a previous study reporting increased truncated TDP-43 in isolated total mitochondria from APP/PS1 transgenic mice lacking robust neurodegeneration [23], we did not note the accumulation of truncated TDP-43 in mitochondria from 5XFAD mice. Noteworthily, truncated TDP-43 does not containing M1 mitochondrial localization sequence [27] and has been reported to be restricted in the intermembrane space without any functional impact on ND3/6 expression or mitochondrial function [21]. Therefore, we do not anticipate the involvement of truncated TDP-43 in neuronal loss and behavioral deficits in 5XFAD mice. Nevertheless, based on the remarkable protective effects of PM1 on Aβ toxicity on neurons in 5XFAD mice, our study strongly suggests an important role of mitochondria-associated TDP-43 in mediating Aβ toxicity. Of note, despite increasing evidence suggesting mitochondria as targets of TDP-43 [21-27], there are considerable discrepancies as to its exact sub-mitochondrial localization and its interaction with different mitochondrial function/pathways. To resolve controversy and further investigate the role of mitochondria-associated TDP-43 in AD and other

neurodegenerative diseases, novel approaches may be needed to test whether mitochondria-associated TDP-43 or TDP-43 fragments synergically mediate Aβ toxicity on mitochondria and neurons through multiple pathways involving but not limited to bioenergetics, mitochondrial dynamics and ER/mitochondria tethering.

5. Conclusions

In summary, the present study provides timely information for understanding the role of TDP-43 proteinopathy, and especially mitochondrial-associated TDP-43 in AD. In addition to mitochondrial dysfunction [61], TDP-43 proteinopathy is a common prominent pathological feature in various major neurodegenerative diseases including AD and related dementias. We believe that in our investigation of mitochondrial TDP-43, its interaction with AD-related neuropathologies and its contribution to neuronal loss and cognitive decline in 5XFAD mice for AD are of broad significance in the field of neurodegeneration. More importantly, PM1 is sufficient to prevent neuron loss and improve cognitive impairment well after symptom onset, suggesting that targeting TDP-43 mitochondrial localization can be a novel therapeutic approach with potentially disease-modifying, rather than symptomatic benefits.

Supplementary Material

Refer to Web version on PubMed Central for supplementary material.

Acknowledgements:

This work was supported by the US National Institutes of Health (RF1AG056320 to X.W.) and the US Alzheimer's Association (AARG-17-499682 to X.W.).

REFERENCE

[1]. Smith MA, Alzheimer disease, International review of neurobiology, 42 (1998) 1–54. [PubMed: 9476170]

[2]. Kwiatkowski TJ Jr., Bosco DA, Leclerc AL, Tamrazian E, Vanderburg CR, Russ C, Davis A, Gilchrist J, Kasarskis EJ, Munsat T, Valdmanis P, Rouleau GA, Hosier BA, Cortelli P, de Jong PJ, Yoshinaga Y, Haines JL, Pericak-Vance MA, Yan J, Ticozzi N, Siddique T, McKenna-Yasek D, Sapp PC, Horvitz HR, Landers JE, Brown RH Jr., Mutations in the FUS/TLS gene on chromosome 16 cause familial amyotrophic lateral sclerosis, Science, 323 (2009) 1205–1208. [PubMed: 19251627]

[3]. Vance C, Rogelj B, Hortobagyi T, De Vos KJ, Nishimura AL, Sreedharan J, Hu X, Smith B, Ruddy D, Wright P, Ganesalingam J, Williams KL, Tripathi V, Al-Saraj S, Al-Chalabi A, Leigh PN, Blair IP, Nicholson G, de Belleroche J, Gallo JM, Miller CC, Shaw CE, Mutations in FUS, an RNA processing protein, cause familial amyotrophic lateral sclerosis type 6, Science, 323 (2009) 1208–1211. [PubMed: 19251628]

[4]. Kabashi E, Valdmanis PN, Dion P, Spiegelman D, McConkey BJ, Vande Velde C, Bouchard JP, Lacomblez L, Pochigaeva K, Salachas F, Pradat PF, Camu W, Meininger V, Dupre N, Rouleau GA, TARDBP mutations in individuals with sporadic and familial amyotrophic lateral sclerosis, Nature genetics, 40 (2008) 572–574. [PubMed: 18372902]

[5]. Neumann M, Sampathu DM, Kwong LK, Truax AC, Micsenyi MC, Chou TT, Bruce J, Schuck T, Grossman M, Clark CM, McCluskey LF, Miller BL, Masliah E, Mackenzie IR, Feldman H, Feiden W, Kretzschmar HA, Trojanowski JQ, Lee VM, Ubiquitinated TDP-43 in frontotemporal

lobar degeneration and amyotrophic lateral sclerosis, Science, 314 (2006) 130–133. [PubMed: 17023659]

[6]. Arai T, Hasegawa M, Akiyama H, Ikeda K, Nonaka T, Mori H, Mann D, Tsuchiya K, Yoshida M, Hashizume Y, Oda T, TDP-43 is a component of ubiquitin-positive tau-negative inclusions in frontotemporal lobar degeneration and amyotrophic lateral sclerosis, Biochem Biophys Res Commun, 351 (2006) 602–611. [PubMed: 17084815]

[7]. Nag S, Yu L, Wilson RS, Chen EY, Bennett DA, Schneider JA, TDP-43 pathology and memory impairment in elders without pathologic diagnoses of AD or FTLD, Neurology, 88 (2017) 653–660. [PubMed: 28087828]

[8]. Nag S, Yu L, Boyle PA, Leurgans SE, Bennett DA, Schneider JA, TDP-43 pathology in anterior temporal pole cortex in aging and Alzheimer's disease, Acta Neuropathol Commun, 6 (2018) 33. [PubMed: 29716643]

[9]. Josephs KA, Whitwell JL, Tosakulwong N, Weigand SD, Murray ME, Liesinger AM, Petrucelli L, Senjem ML, Ivnik RJ, Parisi JE, Petersen RC, Dickson DW, TAR DNA-binding protein 43 and pathological subtype of Alzheimer's disease impact clinical features, Annals of neurology, 78 (2015) 697–709. [PubMed: 26224156]

[10]. Sahoo A, Bejanin A, Murray ME, Tosakulwong N, Weigand SD, Serie AM, Senjem ML, Machulda MM, Parisi JE, Boeve BF, Knopman DS, Petersen RC, Dickson DW, Whitwell JL, Josephs KA, TDP-43 and Alzheimer's Disease Pathologic Subtype in Non-Amnestic Alzheimer's Disease Dementia, J Alzheimers Dis, 64 (2018) 1227–1233. [PubMed: 30010126]

[11]. Josephs KA, Murray ME, Whitwell JL, Tosakulwong N, Weigand SD, Petrucelli L, Liesinger AM, Petersen RC, Parisi JE, Dickson DW, Updated TDP-43 in Alzheimer's disease staging scheme, Acta Neuropathol, 131 (2016) 571–585. [PubMed: 26810071]

[12]. Amador-Ortiz C, Lin WL, Ahmed Z, Personett D, Davies P, Duara R, Graff-Radford NR, Hutton ML, Dickson DW, TDP-43 immunoreactivity in hippocampal sclerosis and Alzheimer's disease, Annals of neurology, 61 (2007) 435–445. [PubMed: 17469117]

[13]. Nelson PT, Dickson DW, Trojanowski JQ, Jack CR, Boyle PA, Arfanakis K, Rademakers R, Alafuzoff I, Attems J, Brayne C, Coyle-Gilchrist ITS, Chui HC, Fardo DW, Flanagan ME, Halliday G, Hokkanen SRK, Hunter S, Jicha GA, Katsumata Y, Kawas CH, Keene CD, Kovacs GG, Kukull WA, Levey AI, Makkinejad N, Montine TJ, Murayama S, Murray ME, Nag S, Rissman RA, Seeley WW, Sperling RA, White Iii CL, Yu L, Schneider JA, Limbic-predominant age-related TDP-43 encephalopathy (LATE): consensus working group report, Brain, 142 (2019) 1503–1527. [PubMed: 31039256]

[14]. Josephs KA, Murray ME, Whitwell JL, Parisi JE, Petrucelli L, Jack CR, Petersen RC, Dickson DW, Staging TDP-43 pathology in Alzheimer's disease, Acta neuropathologica, 127 (2014) 441–450. [PubMed: 24240737]

[15]. James BD, Wilson RS, Boyle PA, Trojanowski JQ, Bennett DA, Schneider JA, TDP-43 stage, mixed pathologies, and clinical Alzheimer's-type dementia, Brain : a journal of neurology, 139 (2016) 2983–2993. [PubMed: 27694152]

[16]. Xu YF, Gendron TF, Zhang YJ, Lin WL, D'Alton S, Sheng H, Casey MC, Tong J, Knight J, Yu X, Rademakers R, Boylan K, Hutton M, McGowan E, Dickson DW, Lewis J, Petrucelli L, Wild-type human TDP-43 expression causes TDP-43 phosphorylation, mitochondrial aggregation, motor deficits, and early mortality in transgenic mice, The Journal of neuroscience : the official journal of the Society for Neuroscience, 30 (2010) 10851–10859. [PubMed: 20702714]

[17]. Wang W, Li L, Lin WL, Dickson DW, Petrucelli L, Zhang T, Wang X, The ALS disease-associated mutant TDP-43 impairs mitochondrial dynamics and function in motor neurons, Human molecular genetics, 22 (2013) 4706–4719. [PubMed: 23827948]

[18]. Magrane J, Cortez C, Gan WB, Manfredi G, Abnormal mitochondrial transport and morphology are common pathological denominators in SOD1 and TDP43 ALS mouse models, Human molecular genetics, 23 (2014) 1413–1424. [PubMed: 24154542]

[19]. Lu J, Duan W, Guo Y, Jiang H, Li Z, Huang J, Hong K, Li C, Mitochondrial dysfunction in human TDP-43 transfected NSC34 cell lines and the protective effect of dimethoxy curcumin, Brain research bulletin, 89 (2012) 185–190. [PubMed: 22986236]

[20]. Stribl C, Samara A, Trumbach D, Peis R, Neumann M, Fuchs H, Gailus-Durner V, Hrabe de Angelis M, Rathkolb B, Wolf E, Beckers J, Horsch M, Neff F, Kremmer E, Koob S, Reichert AS,

Hans W, Rozman J, Klingenspor M, Aichler M, Walch AK, Becker L, Klopstock T, Glasl L, Holter SM, Wurst W, Floss T, Mitochondrial dysfunction and decrease in body weight of a transgenic knock-in mouse model for TDP-43, The Journal of biological chemistry, 289 (2014) 10769–10784. [PubMed: 24515116]

[21]. Salvatori I, Ferri A, Scaricamazza S, Giovannelli I, Serrano A, Rossi S, D'Ambrosi N, Cozzolino M, Giulio AD, Moreno S, Valle C, Carri MT, Differential toxicity of TAR DNA-binding protein 43 isoforms depends on their submitochondrial localization in neuronal cells, Journal of neurochemistry, 146 (2018) 585–597. [PubMed: 29779213]

[22]. Genin EC, Bannwarth S, Lespinasse F, Ortega-Vila B, Fragaki K, Itoh K, Villa E, Lacas-Gervais S, Jokela M, Auranen M, Ylikallio E, Mauri-Crouzet A, Tyynismaa H, Vihola A, Auge G, Cochaud C, Sesaki H, Ricci JE, Udd B, Vives-Bauza C, Paquis-Flucklinger V, Loss of MICOS complex integrity and mitochondrial damage, but not TDP-43 mitochondrial localisation, are likely associated with severity of CHCHD10-related diseases, Neurobiol Dis, 119 (2018) 159–171. [PubMed: 30092269]

[23]. Davis SA, Itaman S, Khalid-Janney CM, Sherard JA, Dowell JA, Cairns NJ, Gitcho MA, TDP-43 interacts with mitochondrial proteins critical for mitophagy and mitochondrial dynamics, Neuroscience letters, 678 (2018) 8–15. [PubMed: 29715546]

[24]. Woo JA, Liu T, Trotter C, Fang CC, De Narvaez E, LePochat P, Maslar D, Bukhari A, Zhao X, Deonarine A, Westerheide SD, Kang DE, Loss of function CHCHD10 mutations in cytoplasmic TDP-43 accumulation and synaptic integrity, Nature communications, 8 (2017) 15558.

[25]. Izumikawa K, Nobe Y, Yoshikawa H, Ishikawa H, Miura Y, Nakayama H, Nonaka T, Hasegawa M, Egawa N, Inoue H, Nishikawa K, Yamano K, Simpson RJ, Taoka M, Yamauchi Y, Isobe T, Takahashi N, TDP-43 stabilises the processing intermediates of mitochondrial transcripts, Sci Rep, 7 (2017) 7709. [PubMed: 28794432]

[26]. Kawamata H, Peixoto P, Konrad C, Palomo G, Bredvik K, Gerges M, Valsecchi F, Petrucelli L, Ravits JM, Starkov A, Manfredi G, Mutant TDP-43 does not impair mitochondrial bioenergetics in vitro and in vivo, Molecular neurodegeneration, 12 (2017) 37. [PubMed: 28482850]

[27]. Wang W, Wang L, Lu J, Siedlak SL, Fujioka H, Liang J, Jiang S, Ma X, Jiang Z, da Rocha EL, Sheng M, Choi H, Lerou PH, Li H, Wang X, The inhibition of TDP-43 mitochondrial localization blocks its neuronal toxicity, Nat Med, 22 (2016) 869–878. [PubMed: 27348499]

[28]. Wang WZ, Arakawa H, Wang LW, Okolo O, Siedlak SL, Jiang YF, Gao J, Xie F, Petersen RB, Wang XL, Motor-Coordinative and Cognitive Dysfunction Caused by Mutant TDP-43 Could Be Reversed by Inhibiting Its Mitochondrial Localization, Mol Ther, 25 (2017) 127–139. [PubMed: 28129109]

[29]. Elder GA, Gama Sosa MA, De Gasperi R, Transgenic mouse models of Alzheimer's disease, The Mount Sinai journal of medicine, New York, 77 (2010) 69–81.

[30]. Wirths O, Bayer TA, Neuron loss in transgenic mouse models of Alzheimer's disease, Int J Alzheimers Dis, 2010 (2010).

[31]. Wang W, Arakawa H, Wang L, Okolo O, Siedlak SL, Jiang Y, Gao J, Xie F, Petersen RB, Wang X, Motor-Coordinative and Cognitive Dysfunction Caused by Mutant TDP-43 Could Be Reversed by Inhibiting Its Mitochondrial Localization, Molecular therapy : the journal of the American Society of Gene Therapy, 25 (2017) 127–139. [PubMed: 28129109]

[32]. Wang W, Zhang F, Li L, Tang F, Siedlak SL, Fujioka H, Liu Y, Su B, Pi Y, Wang X, MFN2 couples glutamate excitotoxicity and mitochondrial dysfunction in motor neurons, The Journal of biological chemistry, 290 (2015) 168–182. [PubMed: 25416777]

[33]. Nunomura A, Perry G, Pappolla MA, Wade R, Hirai K, Chiba S, Smith MA, RNA oxidation is a prominent feature of vulnerable neurons in Alzheimer's disease, J Neurosci, 19 (1999) 1959–1964. [PubMed: 10066249]

[34]. Fujioka H, Tandler B, Hoppel CL, Mitochondrial division in rat cardiomyocytes: an electron microscope study, Anatomical record, 295 (2012) 1455–1461.

[35]. Fujioka H, Moghaddas S, Murdock DG, Lesnefsky EJ, Tandler B, Hoppel CL, Decreased cytochrome c oxidase subunit VIIa in aged rat heart mitochondria: immunocytochemistry, Anatomical record, 294 (2011) 1825–1833.

[36]. Schmidt ML, Robinson KA, Lee VM, Trojanowski JQ, Chemical and immunological heterogeneity of fibrillar amyloid in plaques of Alzheimer's disease and Down's syndrome brains revealed by confocal microscopy, The American journal of pathology, 147 (1995) 503–515. [PubMed: 7639340]

[37]. Newman M, Musgrave IF, Lardelli M, Alzheimer disease: amyloidogenesis, the presenilins and animal models, Biochimica et biophysica acta, 1772 (2007) 285–297. [PubMed: 17208417]

[38]. Kirkitadze MD, Kowalska A, Molecular mechanisms initiating amyloid beta-fibril formation in Alzheimer's disease, Acta biochimica Polonica, 52 (2005) 417–423. [PubMed: 15933761]

[39]. Lambert MP, Velasco PT, Chang L, Viola KL, Fernandez S, Lacor PN, Khuon D, Gong YS, Bigio EH, Shaw P, De Felice FG, Krafft GA, Klein WL, Monoclonal antibodies that target pathological assemblies of A beta, Journal of neurochemistry, 100 (2007) 23–35. [PubMed: 17116235]

[40]. Akiyama H, Barger S, Barnum S, Bradt B, Bauer J, Cole GM, Cooper NR, Eikelenboom P, Emmerling M, Fiebich BL, Finch CE, Frautschy S, Griffin WS, Hampel H, Hull M, Landreth G, Lue L, Mrak R, Mackenzie IR, McGeer PL, O'Banion MK, Pachter J, Pasinetti G, Plata-Salaman C, Rogers J, Rydel R, Shen Y, Streit W, Strohmeyer R, Tooyoma I, Van Muiswinkel FL, Veerhuis R, Walker D, Webster S, Wegrzyniak B, Wenk G, Wyss-Coray T, Inflammation and Alzheimer's disease, Neurobiology of aging, 21 (2000) 383–421. [PubMed: 10858586]

[41]. Oakley H, Cole SL, Logan S, Maus E, Shao P, Craft J, Guillozet-Bongaarts A, Ohno M, Disterhoft J, Van Eldik L, Berry R, Vassar R, Intraneuronal beta-amyloid aggregates, neurodegeneration, and neuron loss in transgenic mice with five familial Alzheimer's disease mutations: potential factors in amyloid plaque formation, The Journal of neuroscience : the official journal of the Society for Neuroscience, 26 (2006) 10129–10140. [PubMed: 17021169]

[42]. O'Leary TP, Robertson A, Chipman PH, Rafuse VF, Brown RE, Motor function deficits in the 12 month-old female 5xFAD mouse model of Alzheimer's disease, Behav Brain Res, 337 (2018) 256–263. [PubMed: 28890389]

[43]. Kimura R, Ohno M, Impairments in remote memory stabilization precede hippocampal synaptic and cognitive failures in 5XFAD Alzheimer mouse model, Neurobiol Dis, 33 (2009) 229–235. [PubMed: 19026746]

[44]. O'Mara S, The subiculum: what it does, what it might do, and what neuroanatomy has yet to tell us, J Anat, 207 (2005) 271–282. [PubMed: 16185252]

[45]. Walker AK, Daniels CM, Goldman JE, Trojanowski JQ, Lee VM, Messing A, Astrocytic TDP-43 pathology in Alexander disease, J Neurosci, 34 (2014) 6448–6458. [PubMed: 24806671]

[46]. Xia Q, Wang H, Hao Z, Fu C, Hu Q, Gao F, Ren H, Chen D, Han J, Ying Z, Wang G, TDP-43 loss of function increases TFEB activity and blocks autophagosome-lysosome fusion, The EMBO journal, 35 (2016) 121–142. [PubMed: 26702100]

[47]. Paolicelli RC, Jawaid A, Henstridge CM, Valeri A, Merlini M, Robinson JL, Lee EB, Rose J, Appel S, Lee VM, Trojanowski JQ, Spires-Jones T, Schulz PE, Rajendran L, TDP-43 Depletion in Microglia Promotes Amyloid Clearance but Also Induces Synapse Loss, Neuron, 95 (2017) 297–308 e296. [PubMed: 28669544]

[48]. Ayala YM, Misteli T, Baralle FE, TDP-43 regulates retinoblastoma protein phosphorylation through the repression of cyclin-dependent kinase 6 expression, Proceedings of the National Academy of Sciences of the United States of America, 105 (2008) 3785–3789. [PubMed: 18305152]

[49]. Liu X, Li D, Zhang W, Guo M, Zhan Q, Long non-coding RNA gadd7 interacts with TDP-43 and regulates Cdk6 mRNA decay, EMBO J, 31 (2012) 4415–4427. [PubMed: 23103768]

[50]. Schwenk BM, Hartmann H, Serdaroglu A, Schludi MH, Hornburg D, Meissner F, Orozco D, Colombo A, Tahirovic S, Michaelsen M, Schreiber F, Haupt S, Peitz M, Brustle O, Kupper C, Klopstock T, Otto M, Ludolph AC, Arzberger T, Kuhn PH, Edbauer D, TDP-43 loss of function inhibits endosomal trafficking and alters trophic signaling in neurons, The EMBO journal, 35 (2016) 2350–2370. [PubMed: 27621269]

[51]. Chiang PM, Ling J, Jeong YH, Price DL, Aja SM, Wong PC, Deletion of TDP-43 down-regulates Tbc1d1, a gene linked to obesity, and alters body fat metabolism, Proceedings of the National Academy of Sciences of the United States of America, 107 (2010) 16320–16324. [PubMed: 20660762]

[52]. Wang X, Fan H, Ying Z, Li B, Wang H, Wang G, Degradation of TDP-43 and its pathogenic form by autophagy and the ubiquitin-proteasome system, Neuroscience letters, 469 (2010) 112–116. [PubMed: 19944744]

[53]. van Eersel J, Ke YD, Gladbach A, Bi M, Gotz J, Kril JJ, Ittner LM, Cytoplasmic accumulation and aggregation of TDP-43 upon proteasome inhibition in cultured neurons, PloS one, 6 (2011) e22850. [PubMed: 21829535]

[54]. Ruan L, Zhou C, Jin E, Kucharavy A, Zhang Y, Wen Z, Florens L, Li R, Cytosolic proteostasis through importing of misfolded proteins into mitochondria, Nature, 543 (2017) 443–446. [PubMed: 28241148]

[55]. Wang P, Deng J, Dong J, Liu J, Bigio EH, Mesulam M, Wang T, Sun L, Wang L, Lee AY, McGee WA, Chen X, Fushimi K, Zhu L, Wu JY, TDP-43 induces mitochondrial damage and activates the mitochondrial unfolded protein response, PLoS Genet, 15 (2019) e1007947. [PubMed: 31100073]

[56]. Mossmann D, Vogtle FN, Taskin AA, Teixeira PF, Ring J, Burkhart JM, Burger N, Pinho CM, Tadic J, Loreth D, Graff C, Metzger F, Sickmann A, Kretz O, Wiedemann N, Zahedi RP, Madeo F, Glaser E, Meisinger C, Amyloid-beta peptide induces mitochondrial dysfunction by inhibition of preprotein maturation, Cell metabolism, 20 (2014) 662–669. [PubMed: 25176146]

[57]. Geissler A, Krimmer T, Bomer U, Guiard B, Rassow J, Pfanner N, Membrane potential-driven protein import into mitochondria - The sorting sequence cytochrome b(2) modulates the Delta psi-dependence of translocation of the matrix-targeting sequence, Mol Biol Cell, 11 (2000) 3977–3991. [PubMed: 11071921]

[58]. Wang X, Su B, Siedlak SL, Moreira PI, Fujioka H, Wang Y, Casadesus G, Zhu X, Amyloid-beta overproduction causes abnormal mitochondrial dynamics via differential modulation of mitochondrial fission/fusion proteins, Proceedings of the National Academy of Sciences of the United States of America, 105 (2008) 19318–19323. [PubMed: 19050078]

[59]. Wang X, Su B, Lee HG, Li X, Perry G, Smith MA, Zhu X, Impaired balance of mitochondrial fission and fusion in Alzheimer's disease, J Neurosci, 29 (2009) 9090–9103. [PubMed: 19605646]

[60]. Schmidt O, Pfanner N, Meisinger C, Mitochondrial protein import: from proteomics to functional mechanisms, Nat Rev Mol Cell Biol, 11 (2010) 655–667. [PubMed: 20729931]

[61]. Lin MT, Beal MF, Mitochondrial dysfunction and oxidative stress in neurodegenerative diseases, Nature, 443 (2006) 787–795. [PubMed: 17051205]

Highlights:

- Mitochondria-associated TDP-43 is increased in AD patients and transgenic mice for AD
- The suppression of mitochondria-associated TDP-43 prevents mitochondrial abnormalities in transgenic mice for AD
- The suppression of mitochondria-associated TDP-43 alleviates neuronal loss in transgenic mice for AD
- The suppression of mitochondria-associated TDP-43 improves the cognitive and motor function in transgenic mice for AD

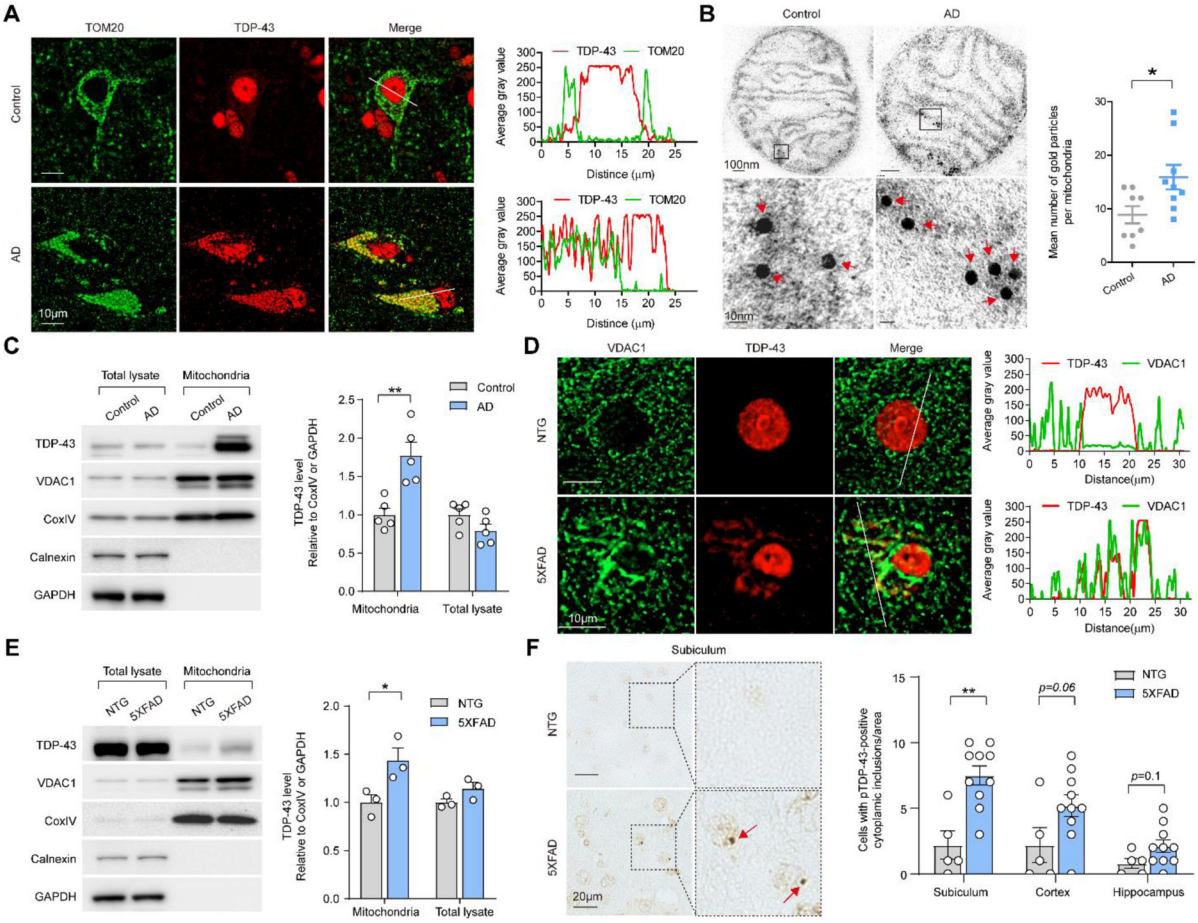

Fig. 1. TDP-43 colocalizes with and accumulates in mitochondria in the brains of AD patients and 5XFAD mice.

(A) Representative images of TOM20 and TDP-43 in human cortical neurons from AD or age-matched healthy individuals. Right, line scan analysis along the solid white lines depicted in the merged images to the left. (B) Immuno-EM of TDP-43 in mitochondria from age-matched healthy control and AD cortex. Red arrowheads, immunogold-labeled TDP-43. Right, quantification using thin EM sections with 50nm thickness (n = 8 mitochondria in control, 9 mitochondria in AD). (C) Representative immunoblot and quantification of TDP-43 levels in sub-mitochondria fractions prepared from age-matched controls (n = 5) or AD cortex (n = 5). (D) Representative images of VDAC1 and TDP-43 in the subiculum neurons of NTG and 5XFAD mice. Right, line scan analysis along the solid white lines depicted in the merged images to the left. (E) Representative immunoblot and quantification of TDP-43 in sub-mitochondrial fractions prepared from the brain of NTG (n = 3) and 5XFAD mice (n = 3). (F) Representative images and quantification of neurons with cytoplasmic pTDP-43-positive inclusions in different brain areas of NTG (n = 5) and 5XFAD mice (n = 10) at 9 months old. Red arrowheads, neurons with cytoplasmic pTDP-43-positive inclusions. Data are means ± s.e.m., representative of triplicate independent experiments. Student's *t*-test. $*P < 0.05$, $**P < 0.01$, $***P < 0.001$.

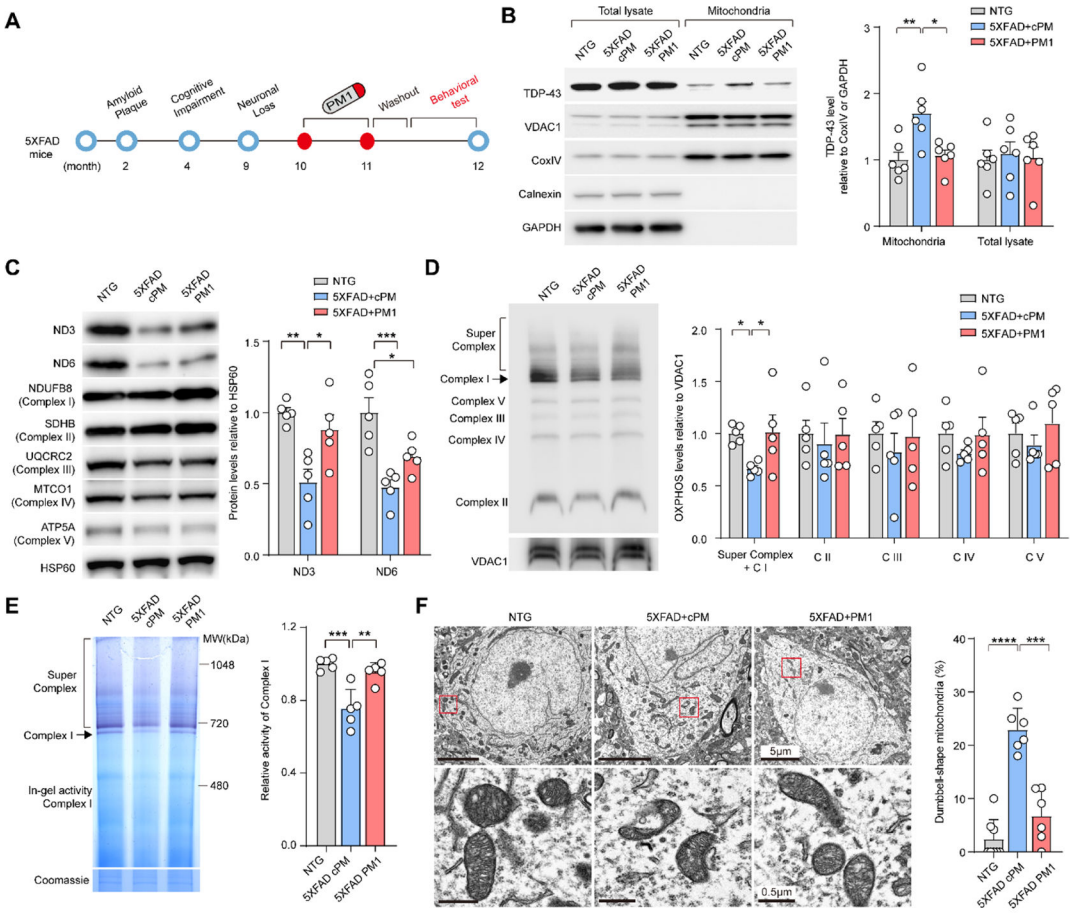

Fig. 2. Inhibition of TDP-43 mitochondrial localization and mitochondrial dysfunction in the brains of 5XFAD mice by PM1.

(A) Schematic model of the progression of the AD-like pathology in 5XFAD mice. Aβ accumulation in 5XFAD mice starts at 2 months of age and the first memory and behavioral deficits in 5XFAD mice appear at about 4 months of age. The obvious neuronal loss in the subiculum occurs at about 9 months of age. 10-month-old 5XFAD mice were treated with PM1 or control peptide cPM (0.5 mg/kg/day continuously, mini osmotic pumps) for 4 weeks. Followed by a two-week washout period, the behavioral tests, quantification of amyloid plaques, and glial reactivity in brain slices were performed. (B) Representative immunoblot and quantification of TDP-43 level in mitochondrial fractions prepared from the brain of NTG (n = 6) and 5XFAD mice treated with PM1 (n = 6) or cPM (n = 6). (C) Representative immunoblot and quantification of OXPHOS complex subunits in mitochondrial fractions prepared from the brain of NTG (n = 5) and 5XFAD mice treated with PM1 (n = 5) or cPM (n = 5). (D) Representative immunoblot and quantification of OXPHOS complex assembly in mitochondrial fractions prepared from the brain of NTG (n = 5) and 5XFAD mice treated with PM1 (n = 5) or cPM (n = 5). (E) In-gel assay of NADH dehydrogenase activity in mitochondrial fractions prepared from the brain of NTG (n=3) and 5XFAD mice treated with PM1 (n = 5) or cPM (n = 5). (F) EM analysis and quantification of mitochondrial morphology change in cortical neurons of NTG (n = 7 neurons) and 5XFAD mice treated with PM1 (n = 6 neurons) or cPM (n = 6 neurons). Data are means ±

s.e.m., representative of triplicate independent experiments. One-way analysis of variance (ANOVA) followed by Tukey's multiple comparison test. *$P < 0.05$, **$P<0.01$.

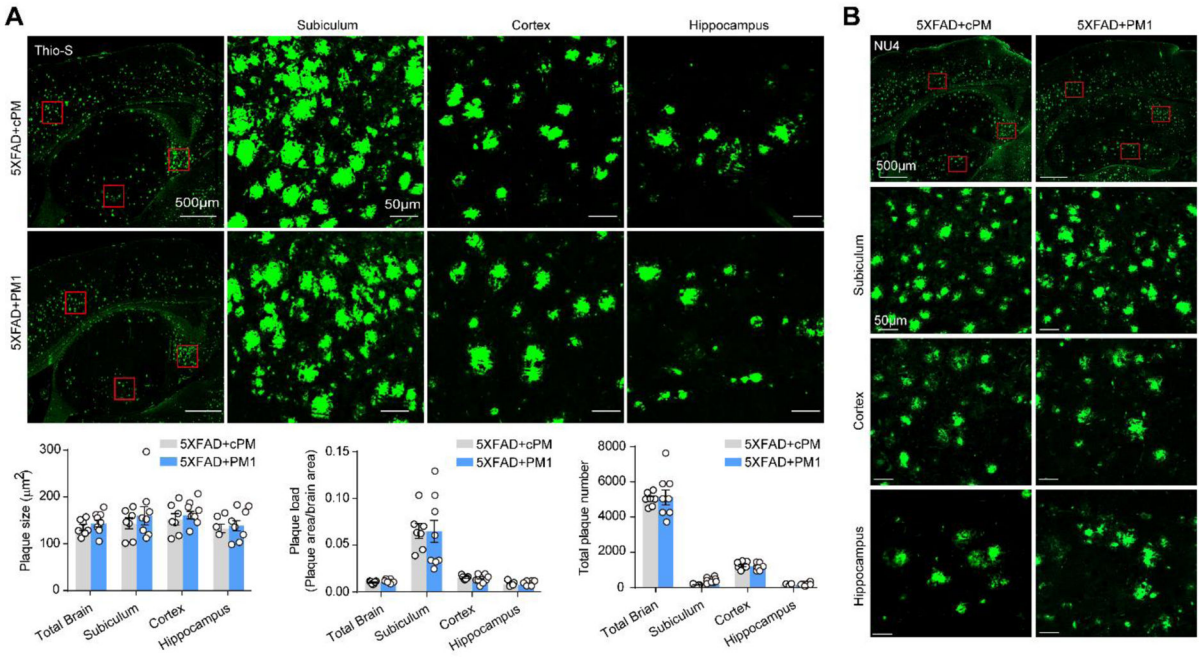

Fig. 3. Blocking TDP-43 mitochondrial accumulation does not modulate Aβ plaque deposition in aged 5XFAD mice.

(A) Representative images of dense core plaques (Thio-S) in the subiculum, cortex, and hippocampus of 5XFAD mice treated with PM1 or cPM. Lower panel showed quantification of number, load, and average area of Thio-S positive plaques in the subiculum, cortex, and hippocampus of PM1 (n = 8) or cPM1 (n = 7) treated 5XFAD mice. (B) Representative images of plaques stained with NU4 antibody in the subiculum, cortex, and hippocampus of 5XFAD mice treated with PM1 or cPM. Data are means ± s.e.m., representative of triplicate independent experiments. Student's *t*-test.

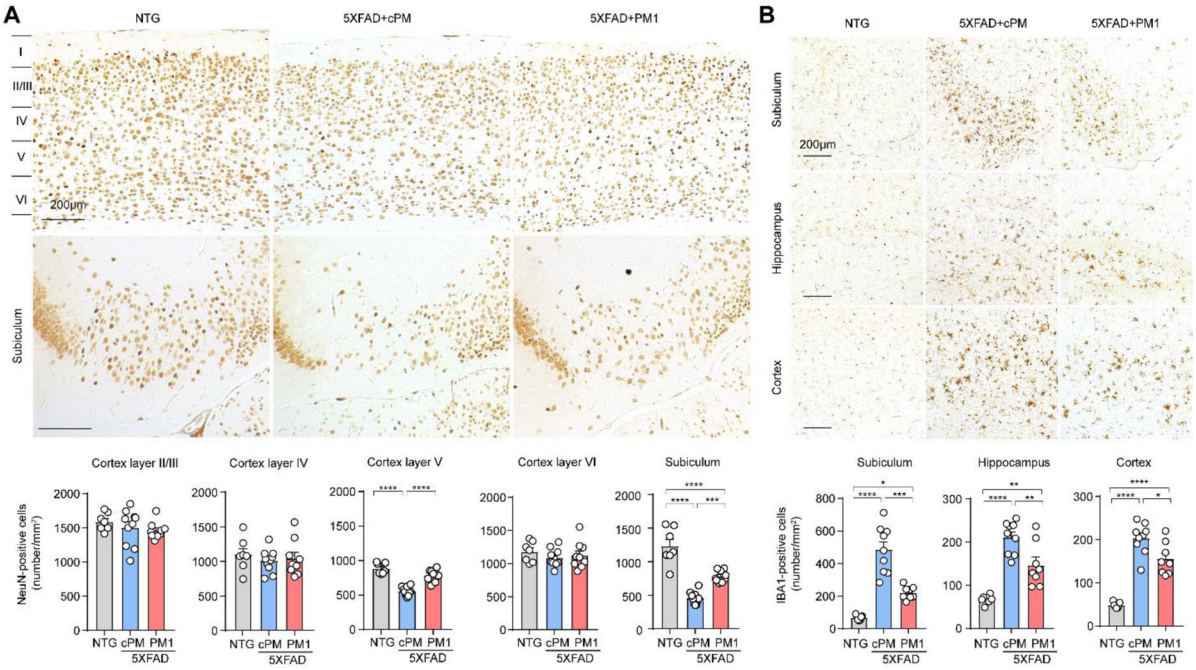

Fig. 4. PM1 prevents neuronal loss and microgliosis in aged 5XFAD mice.

(A) Representative images and quantification of immunohistochemistry staining of NeuN in the subiculum and cortex of NTG (n = 7) and 5XFAD mice treated with PM1 (n = 9) or cPM (n = 9). (B) Representative images and quantification of immunohistochemistry staining of Iba1 in the selected brain areas of NTG (n = 7) and 5XFAD mice treated with PM1 (n = 8) or cPM1 (n = 9). Data are means ± s.e.m., representative of triplicate independent experiments. One-way analysis of variance (ANOVA) followed by Tukey's multiple comparison test. *$P < 0.05$, **$P<0.01$, ***$P<0.001$, ****$p<0.0001$.

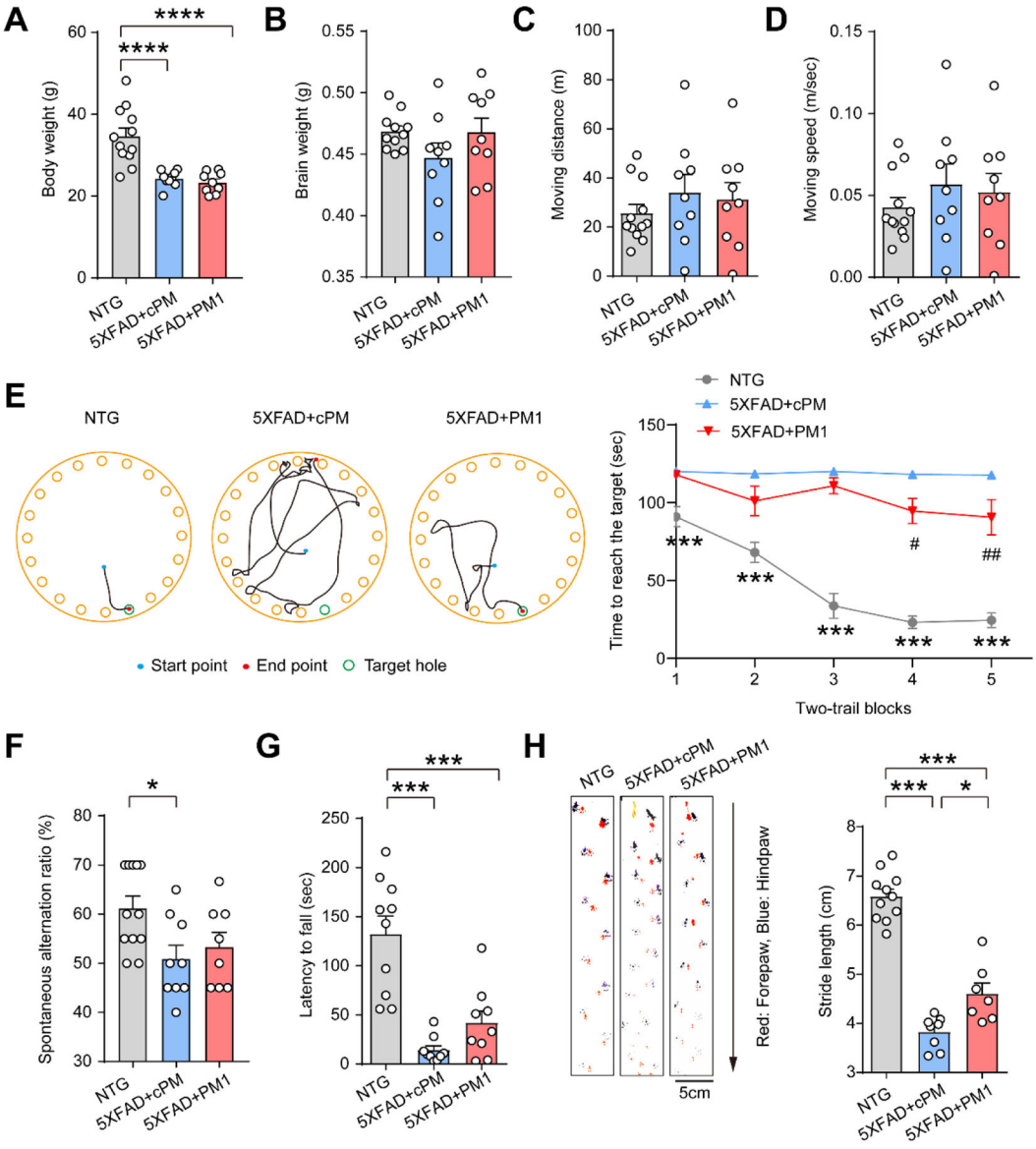

Fig. 5. PM1 improves cognitive and motor function in aged 5XFAD mice.

(A and B), Body weight and brain weight of NTG (n = 12) and 5XFAD mice treated with cPM (n = 9) and PM1 (n = 9). (C and D) The distance traveled and velocity of NTG (n = 12) and 5XFAD mice treated with cPM (n = 9) or PM1 (n = 9), recorded continually for 10 min in open field tests. (E) Representative track plots of NTG and 5XFAD mice treated with PM1 or cPM in the second trial at day 5. Right, representative Barnes maze performance of NTG (n = 11) and 5XFAD mice treated with cPM (n = 9) or PM1 (n = 9) over 5 days of successive testing (two trials/day). (F) Performance in the Y-maze paradigm of NTG (n = 11) and 5XFAD mice treated with cPM (n = 9) or PM1 (n = 9). (G) Rotarod performance of NTG (n = 10) and 5XFAD mice treated with cPM (n = 9) or PM1 (n = 9), shown as the maximum time that mice remained on the accelerating rotating rod. (H) Footprint performance and stride length quantification of NTG (n = 11) or 5XFAD mice treated with cPM (n = 7) or PM1 (n = 8). Arrow shows the walking direction. Data are means ± s.e.m.,

One-way analysis of variance (ANOVA) followed by Tukey's multiple comparison test (a, b, c, d, f, g, h), or two-way ANOVA followed by Bonferroni multiple comparisons (e). *P < 0.05, **P < 0.01. In d, ***P< 0.001, NTG vs 5XFAD+cPM; #P< 0.05, ##P< 0.01, 5XFAD +cPM vs 5XFAD+PM1.

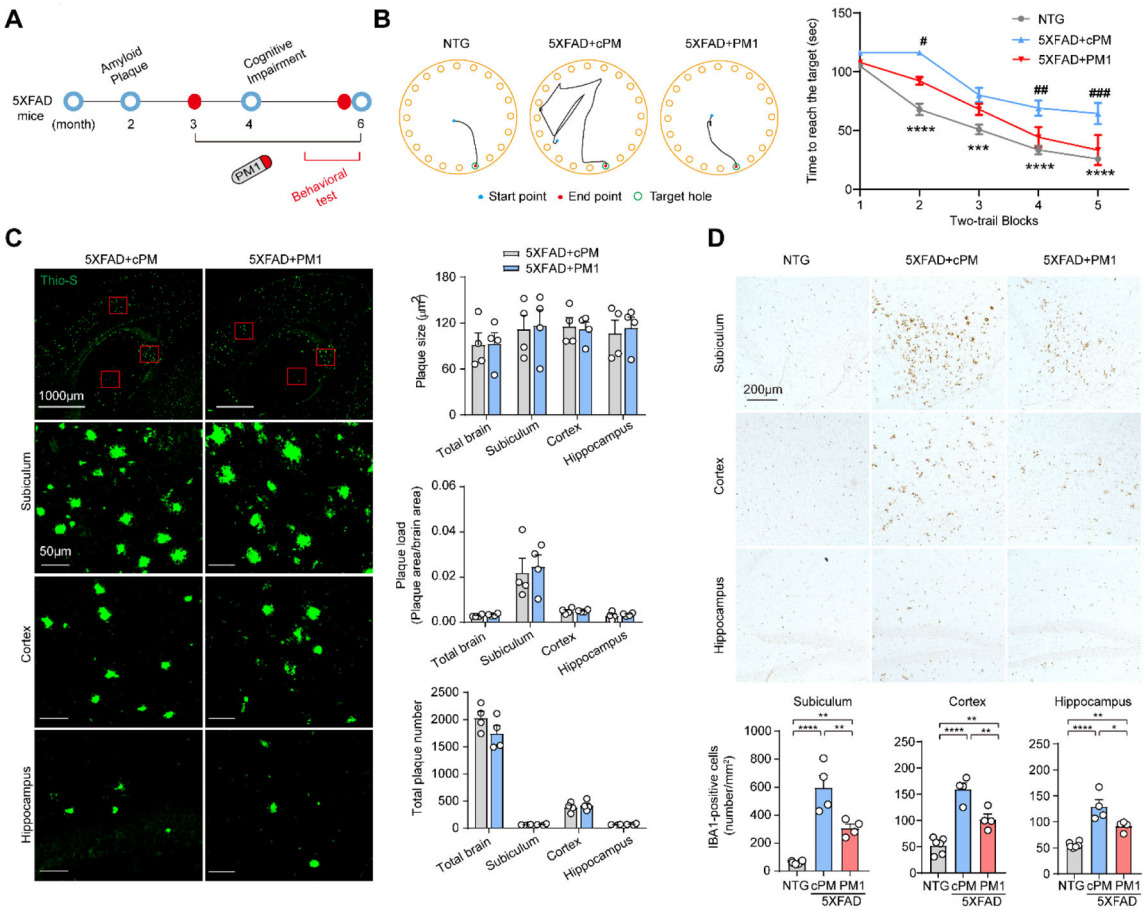

Fig. 6. Prevention of cognitive deficits in young 5XFAD mice by PM1.

(A) Schematic model of disease progression and PM1 treatment proposal in young 5XFAD mice. The first memory and behavioral deficits in 5XFAD mice appear at about 4 months of age. 3-month-old 5XFAD mice were treated with PM1 or control peptide cPM (0.5 mg/kg/day continuously, mini osmotic pumps) for 10 weeks. The behavioral tests were performed at 5 months of age. (B) Representative track plots of NTG and 5XFAD mice treated with PM1 or cPM in the second trial at day 5. Right, representative Barnes maze performance of NTG (n = 21) and 5XFAD mice treated with PM1 (n = 11) or cPM (n = 10) over 5 days of successive testing (two trials/day). (C) Representative images of dense core plaques (Thio-S) in the selected brain areas of 5XFAD mice treated with PM1 (n = 4) or cPM (n = 4). (D) Representative images and quantification of immunohistochemistry staining of Iba1 in the selected brain areas of NTG (n = 7) and 5XFAD mice treated with PM1 (n = 8) or cPM1 (n = 9). Data are means ± s.e.m., two-way ANOVA followed by Bonferroni multiple comparisons (b), Student t-test(c), or one-way analysis of variance (ANOVA) followed by Tukey's multiple comparison test (d), or. $^{**}P < 0.01$, $^{***}P < 0.001$. In b, $^{***}P < 0.001$, NTG vs 5XFAD+cPM; $^{\#}P < 0.05$, $^{\#\#}P < 0.01$, 5XFAD+cPM vs 5XFAD +PM1.